ACS APPLIED MATERIALS & INTERFACES

Research Article

www.acsami.org

Improvement of Cycling Performance of Lithium–Sulfur Batteries by Using Magnesium Oxide as a Functional Additive for Trapping Lithium Polysulfide

Rubha Ponraj, Aravindaraj G. Kannan, Jun Hwan Ahn, and Dong-Won Kim*

Department of Chemical Engineering, Hanyang University, Seoul 133-791, Korea

Supporting Information

ABSTRACT: Trapping lithium polysulfides formed in the sulfur positive electrode of lithium–sulfur batteries is one of the promising approaches to overcome the issues related to polysulfide dissolution. In this work, we demonstrate that intrinsically hydrophilic magnesium oxide (MgO) nanoparticles having surface hydroxyl groups can be used as effective additives to trap lithium polysulfides in the positive electrode. MgO nanoparticles were uniformly distributed on the surface of the active sulfur, and the addition of MgO into the sulfur electrode resulted in an increase in capacity retention of the lithium–sulfur cell compared to a cell with pristine sulfur electrode. The improvement in cycling stability was attributed to the strong chemical interactions between MgO and lithium polysulfide species, which suppressed the shuttling effect of lithium polysulfides and enhanced the utilization of the sulfur active material. To the best of our knowledge, this report is the first demonstration of MgO as an effective functional additive to trap lithium polysulfides in lithium–sulfur cells.

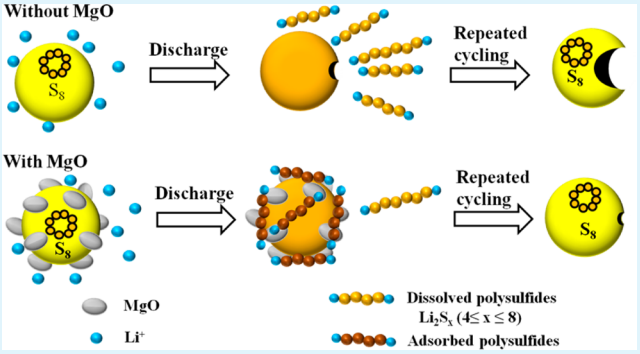

KEYWORDS: *lithium–sulfur battery, magnesium oxide, lithium polysulfide, functional additive, polysulfide dissolution*

INTRODUCTION

Lithium-ion batteries (LIBs) have been the most dominant power sources for portable electronic devices for two decades, and the growing demand for higher energy density applications such as electric vehicles and grid-scale energy storage systems requires great improvement in the energy density of current LIBs.[1−3] Lithium–sulfur batteries have a higher theoretical energy density than that of conventional LIBs and are therefore considered as one of the most promising candidates for future batteries.[4−7] Moreover, lithium–sulfur batteries are environmentally friendly and are cost-competitive due to the natural abundance of sulfur.[8,9] However, practical applications of lithium–sulfur batteries are still hindered by the low utilization of sulfur, poor cycling stability and poor rate capability. These problems are mainly due to the following issues: (a) the poor electronic conductivity of sulfur and discharge products, (b) the high volume expansion upon lithiation of sulfur to form Li_2S, which leads to capacity fading during cycling, and (c) dissolution of intermediate lithium polysulfides (Li_2S_x, $4 \le x \le 8$) into the electrolyte solution, which triggers a polysulfide shuttle process and results in low Coulombic efficiency, loss of active material and poor cycle life.[4,9,10] Various methods to address these issues have been reported including modifying the electrode to confine the lithium polysulfides within the sulfur positive electrode,[11,12] improving electronic conductivity using a conductive matrix,[13−17] directly utilizing Li_2S in the cathode,[18] modifying the separators to mitigate shuttle effects,[19] using carbon-based anodes,[20] optimizing the electrolyte composition to suppress the dissolution of polysulfides into the electrolyte solution,[21] and protecting the Li electrode to minimize the shuttle effect.[22−24] Among these approaches, physically trapping lithium polysulfides within the electrode by encapsulating sulfur particles has been widely pursued using various carbonaceous materials such as porous carbon, carbon spheres, carbon nanotubes, carbon fibers and conductive polymers.[13,14,25−35] However, these methods result in weak physical interactions with lithium polysulfides and could only minimize the dissolution/migration of polysulfides to some extent due to the change in morphology that arises from the 80% volume expansion of the sulfur electrode on discharge.[36] Therefore, chemical interactions are required to effectively trap the polysulfides in the positive electrode. This was successfully demonstrated using two-dimensional materials such as graphene oxide and amino functionalized graphene oxide, where the polysulfide interacted with oxygen and amino-functional groups, respectively.[37−40] Another promising approach employed in previous studies is the addition of hydrophilic and polar host oxide materials such as mesoporous

Received: November 23, 2015
Accepted: January 25, 2016
Published: January 25, 2016

DOI: 10.1021/acsami.5b11327
ACS Appl. Mater. Interfaces 2016, 8, 4000–4006

SiO_2, Al_2O_3, TiO_2, Ti_4O_7, and MnO_2 in the sulfur positive electrode, which effectively trapped the polysulfides.[41−48]

In this study, a simple and facile method is reported to confine lithium polysulfide in the sulfur positive electrode, as schematically illustrated in Figure 1. Magnesium oxide (MgO) nanoparticles were used as functional additives to chemically bind the lithium polysulfide within the positive electrode to enhance the cycling stability of lithium−sulfur cells. Considering the hydrophilic nature of MgO nanoparticles and the presence of hydroxyl groups on MgO surface,[49−51] we expected that polysulfide would be effectively adsorbed onto the MgO. In addition, magnesium metal is more electropositive than the previously studied transition metals such as Ti and Mn, which would facilitate strong chemical binding with lithium polysulfides. As a result, lithium−sulfur cells with a small amount of MgO in the sulfur positive electrode exhibited better capacity retention and higher Coulombic efficiency than lithium−sulfur cell with pristine sulfur because of the effective suppression of polysulfide dissolution. The detailed mechanism of lithium polysulfide binding by MgO nanoparticle was elucidated using X-ray photoelectron spectroscopic (XPS) analysis.

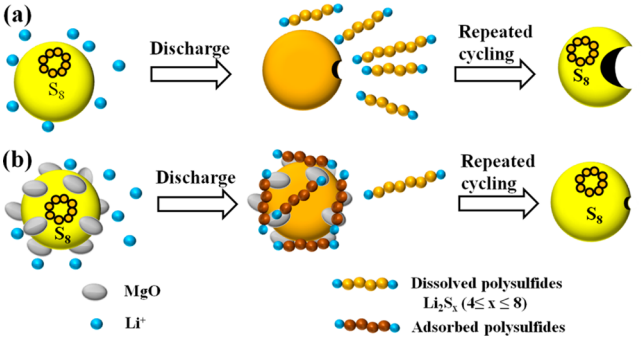

Figure 1. Schematic illustration of the adsorption of lithium polysulfide on the surface of a MgO nanoparticle. (a) For a pristine sulfur electrode without MgO, dissolution of lithium polysulfide into the electrolyte occurs upon lithiation, and sulfur is gradually lost with repeated cycling. (b) For a sulfur electrode with MgO as an adsorbent, lithium polysulfides are adsorbed on the MgO surface upon lithiation and are retained within the positive electrode, resulting in stable cycling performance.

EXPERIMENTAL SECTION

Preparation of the SMgO Composites. A mixture of MgO nanoparticles (Sigma-Aldrich) and elemental sulfur (Sigma-Aldrich) in different ratios was dispersed in ethanol and was ball-milled for 2 h at 600 rpm. The resulting mixture was then dried at 60 °C overnight to remove the ethanol solvent. Three different compositions of SMgO composites with S:MgO weight ratios of 95:5, 90:10, and 80:20 were prepared using the above procedure, and these will be designated hereafter as SMgO-5, SMgO-10, and SMgO-20, respectively.

Synthesis of Lithium Polysulfide (Li_2S_4) and MgO-Li_2S_4 for Studying Polysulfide Adsorption. Lithium polysulfide was synthesized according to the procedure reported by Nazar et al.[47] In a typical preparation, sulfur and 1 M lithium triethylborohydride in tetrahydrofuran (THF) (superhydride solution, Sigma-Aldrich) were mixed in a molar ratio of 1:2.75 until the sulfur was completely dissolved. The solution was dried under vacuum to obtain a yellow product followed by final washing with toluene to remove the unreacted substances. The precipitate was dried in a vacuum oven and a fine yellow powder (Li_2S_4) was finally obtained. Then, 5 mg of Li_2S_4 was dissolved in 5 mL of THF (Sigma-Aldrich), and 40 mg of MgO was added into the solution followed by stirring for 1 h. The solution was allowed to settle, and the precipitated product was dried in vacuum to obtain MgO-Li_2S_4 for XPS analysis. All the procedures were carried out in an Ar-filled glovebox.

Electrode Preparation and Cell Assembly. The positive electrode was prepared by coating an *N*-methyl-2-pyrrolidone (NMP)-based slurry containing 60 wt % SMgO composite (SMgO-5, SMgO-10 and SMgO-20), 30 wt % super-P carbon (MMM Co.) and 10 wt % poly(vinylidene fluoride) (PVdF) onto aluminum foil. The pristine sulfur cathode was prepared as a control sample in a similar manner without using MgO additive. The mass loading of the active sulfur in the positive electrode was about 1.8−2.0 mg cm^{-2}. The negative electrode consisted of a 100 μm thick lithium foil (Honjo Metal Co. Ltd.) pressed onto a copper current collector. A CR2032-type coin cell was assembled by sandwiching the polyethylene separator (Asahi ND 420) between the lithium negative electrode and the sulfur positive electrode. The cell was then injected with an electrolyte solution consisting of 1 M lithium bis-(trifluoromethanesulfonyl)imide ($LiN(SO_2CF_3)_2$, LiTFSI) in a mixed solvent of 1,3-dioxalane (DOL) and 1,2-dimethoxyethane (DME) (50/50 by volume) including 2 wt % $LiNO_3$ as an electrolyte additive. All cells were assembled in a drybox filled with argon gas.

Characterization and Measurements. Scanning electron microscope (SEM, JEOL JSM 6701F) analyses were performed to investigate the morphology of MgO nanoparticles and SMgO composites. Energy dispersive X-ray spectroscopy (EDX) mapping was used for surface elemental characterization of the SMgO composites. XPS spectra were obtained to investigate the interactions between MgO nanoparticles and lithium polysulfides using a VG multilab ESCA 220i system. Samples were loaded using a sealed tube filled with Ar in the glovebox and were quickly transferred to the XPS vacuum chamber. All spectra were fitted with a Gaussian peak fit function and a Shirley-type background. X-ray diffraction (XRD) patterns of the materials were recorded in the 2θ range from 10 to 70° using a Rigaku D/MAX 2500 diffractometer. Thermogravimetric analysis (TGA) was carried out on a Mettler Toledo SDTQ600 instrument with a heating rate of 10 °C min^{-1} from room temperature to 1000 °C to determine the sulfur content in the SMgO composites. AC impedance measurements were conducted using a Zahner Electrik IM6 impedance analyzer in the frequency range of 5 mHz to 100 kHz with an AC voltage amplitude of 5 mV. Charge and discharge cycling tests of the lithium−sulfur cells were carried out at 0.2C rate over a voltage range of 1.5 to 3.0 V at 25 °C using battery test equipment (WBCS 3000, WonA Tech Co., Ltd.). Cyclic voltammograms were obtained using a Zahner Electrik IM6 potentiostat in the potential range of 1.5 to 3.0 V at a scan rate of 0.5 mV s^{-1}.

RESULTS AND DISCUSSION

The SMgO composites were prepared by ball-milling a mixture of sulfur and MgO nanoparticles in three different compositions, and the morphologies of the resulting SMgO composites were characterized by SEM (Figure 2). Figure 2a shows that the MgO nanoparticles have an average particle size of about 50

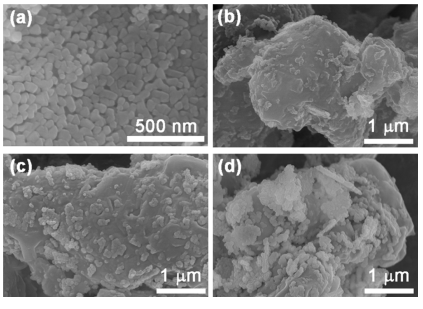

Figure 2. SEM images of (a) MgO nanoparticles, (b) SMgO-5, (c) SMgO-10, and (d) SMgO-20 composites.

DOI: 10.1021/acsami.5b11327
ACS Appl. Mater. Interfaces 2016, 8, 4000−4006

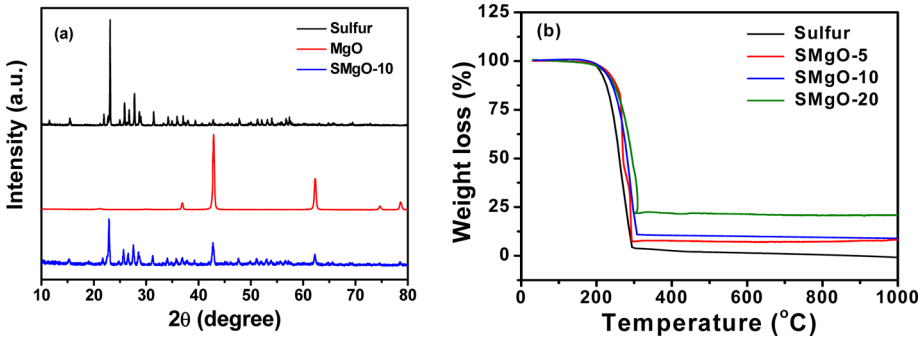

Figure 3. (a) X-ray diffraction patterns of S, MgO nanoparticles, and SMgO-10 composite. (b) TGA curves of sulfur and SMgO composites.

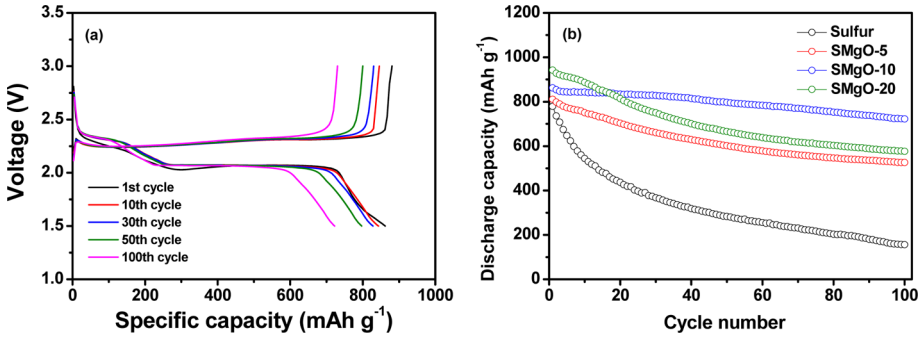

Figure 4. (a) Charge and discharge curves of the lithium−sulfur cell with SMgO-10 composite at 0.2*C* rate, and (b) discharge capacities of the lithium−sulfur cells with pristine sulfur, SMgO-5, SMgO-10, and SMgO-20 composites at 0.2*C* rate as a function of cycle number.

nm. For the SMgO-5 composite, MgO nanoparticles were randomly and sparsely distributed on the surface of the micrometer-sized sulfur particles. The amount of MgO nanoparticles was not sufficient to cover the surface of the sulfur in SMgO-5, and therefore trapping of polysulfides in the electrode was not expected to be efficient (Figure 2b). In contrast, MgO nanoparticles were uniformly dispersed on the surface of active sulfur in the SMgO-10 composite, and this composite showed good contact between sulfur and MgO nanoparticles (Figure 2c). To further confirm the uniform distribution of MgO nanoparticles on the surface of the sulfur, EDX elemental maps of sulfur, magnesium and oxygen atoms in the SMgO-10 composite were obtained (Figure S1). As shown in figure, Mg and O were uniformly distributed on the surface of the sulfur, which was in good agreement with the SEM result. In the case of the SMgO-20 composite (Figure 2d), the agglomeration of MgO nanoparticles was observed throughout the surface of the sulfur particles, indicating that the amount of MgO was too high to obtain a uniform distribution of MgO nanoparticles on the surface of the sulfur.

XRD patterns of pristine sulfur, MgO and SMgO composite (SMgO-10) are presented in Figure 3a. The diffraction pattern of pristine sulfur showed crystalline peaks matching those of the standard orthorhombic sulfur (JCPDS no. 08−0247).[42] The XRD pattern of MgO nanoparticles was crystalline in nature, and corresponded well with JCPDS no. 45−0946.[52] The XRD pattern of the SMgO composite showed crystalline peaks corresponding to both MgO and pristine sulfur, indicating that MgO nanoparticles were present on the surface of the sulfur, and the crystalline structure of the sulfur in the SMgO composite was maintained after the ball-milling process. The amount of sulfur in the various SMgO composites was determined from the TGA curves of sulfur and SMgO composites shown in Figure 3b. Sulfur was completely decomposed around 300 °C, and the sulfur contents in the SMgO-5, SMgO-10, and SMgO-20 composites were calculated to be 93, 90, and 80 wt %, respectively.

To confirm that the MgO nanoparticles are electrochemically inactive in the potential range of 1.5 to 3.0 V, the cyclic voltammograms of the SMgO-10 and MgO electrodes were examined, and the results are shown in Figure S2. The SMgO-10 electrode exhibits two peaks in the cathodic scan. These peaks are typical of a sulfur-based electrode, where the peak at higher potential is attributed to the reaction of cyclic sulfur with lithium ions to form soluble long-chain polysulfides (Li_2S_X, $4 \leq X \leq 8$), followed by the formation of insoluble lithium sulfides (Li_2S_2/Li_2S) at 2.0 V.[9] During the anodic scan, a broad and overlapped peak is observed, which corresponds to the conversion of discharge products to cyclic sulfur. In contrast, the MgO electrode without sulfur does not show any redox peaks, indicating that the MgO nanoparticles are electrochemically stable and does not directly contribute to the specific capacity of the SMgO composite electrodes. The lithium−sulfur cells assembled with different cathode materials were initially subjected to a preconditioning discharge cycle to 1.5 V at 0.05C rate before cycling tests, and the resulting discharge voltage profiles are shown in Figure S3. The contents of active sulfur in the positive electrodes prepared with the pristine sulfur, SMgO-5, SMgO-10, and SMgO-20 composites were determined to be 60.0, 55.8, 54.0, and 48.0 wt %, respectively, with an active sulfur mass loading of 1.8−2.0 mg cm^{-2} in the positive electrode. The specific capacities of the lithium−sulfur cells were calculated based on the mass of active sulfur in the electrode. We found that the lithium−sulfur cells assembled with SMgO composites exhibited higher discharge capacities than the cell with pristine sulfur, and the discharge capacity increased with increasing MgO content in the SMgO composite. This result can be ascribed to the adsorption of

DOI: 10.1021/acsami.5b11327
ACS Appl. Mater. Interfaces 2016, 8, 4000−4006

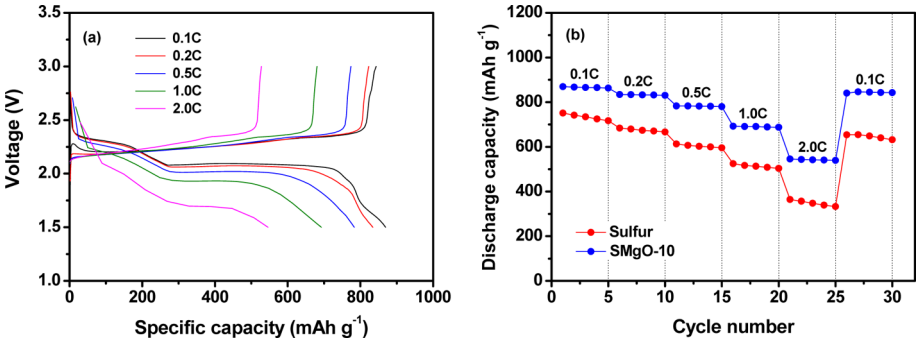

Figure 5. (a) Charge and discharge curves of the lithium−sulfur cell assembled with SMgO-10 composite at various C rates, and (b) rate capability of the lithium−sulfur cells with pristine sulfur and SMgO-10 composite.

soluble lithium polysulfides by MgO nanoparticles, which allows a higher amount of longer chain polysulfides to be formed prior to the electrolyte saturation with soluble polysulfides. This assumption was confirmed based on the fact that the upper discharge plateau was the longest in the cell with SMgO-20 composite electrode, indicating that a higher amount of longer-chain polysulfides was formed. Accordingly, the lithium−sulfur cell with SMgO-20 composite delivered the highest discharge capacity of 1090.3 mAh g^{-1}. After the preconditioning cycle, the cells were cycled in the potential range of 1.5−3.0 V at 0.2*C* rate. The typical charge and discharge curves of the lithium−sulfur cell assembled with SMgO-10 composite are presented in Figure 4a. The charge and discharge voltage profiles display two discharge plateaus at around 2.2 and 2.0 V, and two overlapping charge plateaus at around 2.3 V, which are consistent with the cyclic voltammetry results. The cell delivered an initial discharge capacity of 862.0 mAh g^{-1} and exhibited stable cycling characteristics.

The cycling performance of the lithium−sulfur cells with pristine sulfur, SMgO-5, SMgO-10 and SMgO-20 composites are compared in Figure 4b. As shown, the lithium−sulfur cell with pristine sulfur suffered from rapid capacity decay showing capacity retention of 20.0% after 100 cycles, which may be due to the dissolution of lithium polysulfides into the electrolyte solution during cycling. In contrast, the lithium−sulfur cells with SMgO composites showed higher initial discharge capacities and more stable cycling characteristics than the cell with pristine sulfur. The cell with SMgO-10 composite exhibited the best cycling stability among the cells investigated. The enhanced cycling performance in the cell with a SMgO-10 composite could be attributed to the favorable morphology of the SMgO-10 composite wherein MgO nanoparticles were uniformly distributed on the surface of the sulfur, which allowed effective trapping of lithium polysulfides in the positive electrode during cycling. Although lithium polysulfides could also be trapped in the SMgO-20 composite, only the MgO in direct contact with the sulfur surface could be utilized to form Li_2S_2 and Li_2S. This may result from the fewer electronic conductive pathways caused by the agglomeration of MgO nanoparticles, as evidenced from the SEM image in Figure 2d. The cell with a SMgO-5 composite showed less stable cycling behavior than the cell with SMgO-10 composite, indicating that the amount of MgO in SMgO-5 was too low to effectively trap the lithium polysulfides in the positive electrode. Based on these results, we concluded that the optimum content of MgO nanoparticles to obtain the best cycling stability was 10 wt % in the SMgO composite. Further, the sulfur content was kept constant (54 wt %) and the amount of MgO was varied (3, 6, and 9 wt %) to eliminate any possible effects from the amount of sulfur in the electrode. The cycling results of the lithium−sulfur cells with different amount of MgO at fixed sulfur content are presented in Figure S4. All the composite electrodes exhibited higher discharge capacity and better capacity retention compared to the pristine sulfur electrode. However, the excessive addition of MgO gave an adverse effect on the cycling stability due to the reduction of electronic conductivity and the agglomeration of MgO nanoparticles in the composite electrode. It should be noted that the composite electrode with a composition of S:MgO = 54:6 corresponds to SMgO-10. Figure S5 shows the Coulombic efficiencies of the lithium−sulfur cells assembled with different electrodes. The cell with SMgO-10 composite exhibited higher Coulombic efficiency than the cells with pristine sulfur and other SMgO composites. The irreversible capacity of lithium−sulfur cells was mainly associated with the shuttle reaction of lithium polysulfides.[9] Thus, the higher Coulombic efficiency in the cell with SMgO-10 suggests that the addition of 10 wt % MgO nanoparticles in the sulfur composite can suppress the shuttle reaction of lithium polysulfides by effectively binding the lithium polysulfides to the positive electrode.

The rate capability of the lithium−sulfur cell assembled with SMgO-10 composite electrode at various *C* rates was evaluated, and the corresponding charge and discharge voltage profiles are shown in Figure 5a. As shown, the overpotential increased with increasing current rate. In addition, the upper and lower discharge plateaus were shortened, indicating that the electrochemical reaction was limited by both electronic conductivity and ionic diffusivity at higher rates. We attributed this result to the highly insulating nature of sulfur and the discharge products along with the slow diffusion kinetics of lithium ions in sulfur. The rate performances of the lithium−sulfur cells assembled with pristine sulfur and SMgO-10 composite are compared in Figure 5b. An improvement in rate performance was clearly observed in the cell with the SMgO-10 composite. This result could be attributed to the enhanced charge transfer reaction at the interface due to the addition of MgO nanoparticles, which is consistent with the previous report that the addition of metal oxides as additives into the sulfur cathode reduced the charge transfer resistance.[45] The cell with SMgO-10 also exhibited an ability to recover its capacity when the C rate was decreased from 2.0 to 0.1C. These results demonstrate that the addition of MgO nanoparticles not only increased the cycling stability but also enhanced the rate capability of the lithium−sulfur cell. To understand the reason for the improved rate capability in the cell with SMgO-10, we performed AC impedance measurements in the cells with pristine sulfur and SMgO-10;

DOI: 10.1021/acsami.5b11327
ACS Appl. Mater. Interfaces 2016, 8, 4000−4006

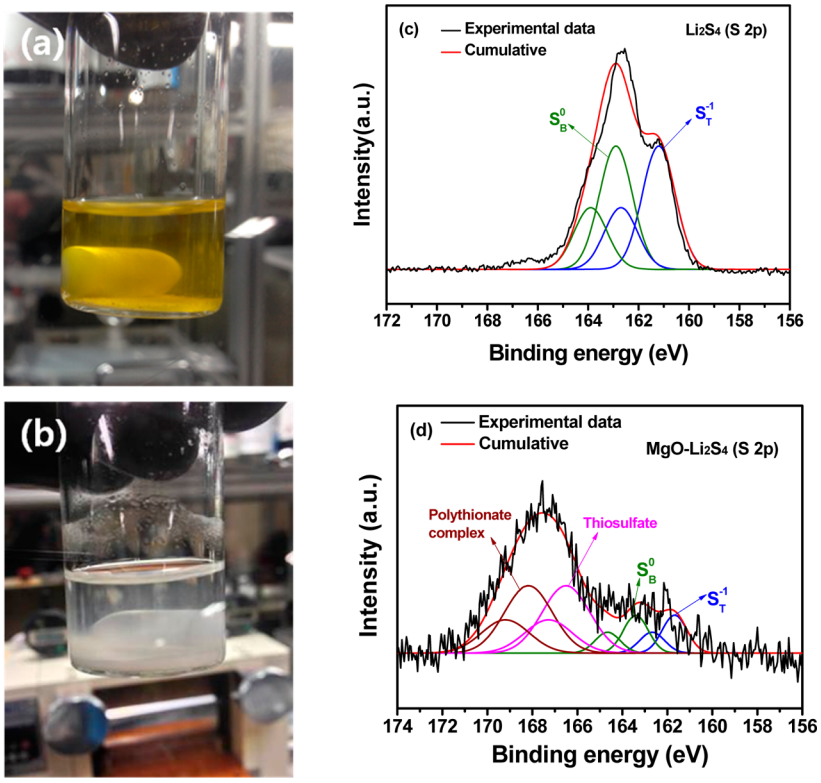

Figure 6. Photographs of Li_2S_4 solution in THF (a) immediately after adding MgO nanoparticles and (b) after stirring with MgO nanoparticles for 1 h. High resolution S 2p XPS spectra of (c) as-prepared Li_2S_4 and (d) MgO-Li_2S_4 mixture obtained after stirring with MgO nanoparticles for 1 h.

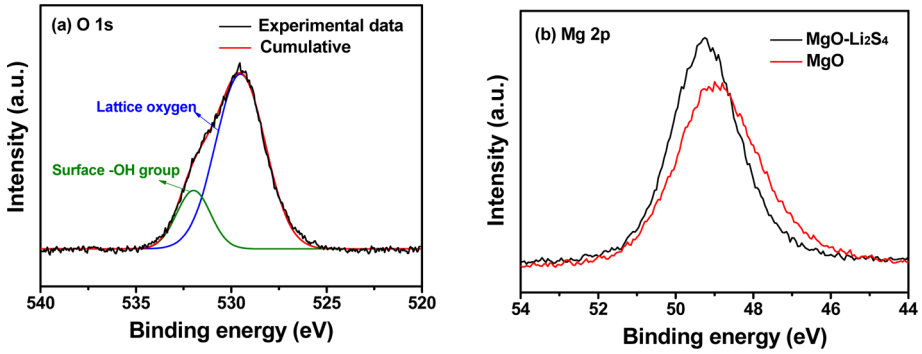

Figure 7. (a) XPS O 1s spectra of MgO nanoparticles showing surface hydroxyl groups, and (b) XPS Mg 2p spectra of MgO nanoparticles and MgO-Li_2S_4 mixture.

these results are shown in Figure S6. The measurements were carried out in fresh cells at open circuit potential so that we could neglect the effect of the solid electrolyte interphase (SEI). As shown in the figure, both cells exhibited similar electrolyte resistance values (R_E) including electrode contact resistance in the high frequency region. A noticeable difference was observed in the charge transfer resistance (R_{ct}) at the electrode and electrolyte interface in the medium-to-low frequency range. The cell with the SMgO-10 composite showed a much lower charge transfer resistance than the cell with pristine sulfur, indicating that the charge transfer reaction was enhanced by addition of MgO nanoparticles.

We also investigated the interactions between lithium polysulfides and MgO nanoparticles, and the results are presented in Figure 6. MgO nanoparticles were mixed with Li_2S_4 solution to simulate the same environment that they would experience in the sulfur positive electrode with MgO additive. The Li_2S_4 solution was initially dark yellow in color (Figure 6a), and the solution became clear and transparent after stirring for 1 h in the presence of MgO nanoparticles (Figure 6b), indicating that the MgO nanoparticles effectively adsorbed the lithium polysulfide. XPS analysis was performed in order to examine the types of interactions between MgO and Li_2S_4. High-resolution S 2p XPS spectra of Li_2S_4 and Li_2S_4-adsorbed MgO nanoparticles are shown in Figures 6c, d, respectively. The deconvoluted XPS spectrum of Li_2S_4 showed two S $2p_{3/2}$ contributions at 161.3 and 162.9 eV, which were assigned to terminal (S_T^{-1}) and bridging sulfur (S_B^0) atoms, respectively. This observation is consistent with spectra of lithium polysulfides reported in previous studies.[47,48] In contrast, the S 2p XPS spectrum of the MgO-Li_2S_4 mixture was quite different, revealing four different sulfur environments. Two peaks were attributed to Li_2S_4 with terminal and bridging sulfur peaks at 161.6 and 163.3 eV, respectively. In addition to these,

DOI: 10.1021/acsami.5b11327
ACS Appl. Mater. Interfaces 2016, 8, 4000−4006

two more peaks were observed at 166.8 and 168.2 eV, which were assigned to thiosulfate and polythionate complexes, respectively, resulting from the strong interactions between MgO and Li_2S_4.[48]

The formation of thiosulfate could be attributed to the presence of OH groups on the surface of hydrophilic MgO, which was confirmed by the XPS analysis. The O 1s spectrum (Figure 7a) shows deconvoluted peaks at 529.5 and 532 eV, which could be assigned to the lattice oxygen component and the surface − OH groups, respectively, based on the previously reported values for commercial MgO particles.[53] An insoluble polythionate complex could be formed by the catenation reaction, and this complex acts as a transfer mediator for Li_2S_2 and Li_2S. To further support the strong interaction between MgO and Li_2S_4, XPS Mg 2p spectra of both MgO nanoparticles and the MgO-Li_2S_4 mixture were analyzed (Figure 7b). A small shift of 0.2 eV to a higher binding energy was observed after the interaction of Li_2S_4 with MgO. This result can be attributed to the electropositive nature of magnesium, which forces electrons away from the metal core because of the presence of a polysulfide environment,[45] resulting in a slight increase in the binding energy.

CONCLUSIONS

We demonstrated that the hydrophilic MgO nanoparticles uniformly distributed on the surface of sulfur could increase the cycling stability of lithium−sulfur cells by confining the lithium polysulfides to the positive electrode. Two mechanisms were suggested for the strong interactions between MgO nanoparticles and polysulfides: (i) the presence of surface hydroxyl groups on MgO nanoparticles resulting in the formation of intermediate insoluble species such as thiosulfate and polythionate complexes, which could bind the soluble polysulfides and promote the formation of insoluble lithium sulfide, and (ii) the presence of more electropositive centered Mg sites resulting in increased binding energy after the interaction of MgO with polysulfides. Because of these strong interactions, the lithium−sulfur cell with SMgO-10 composite demonstrated the best cycling performance with capacity retention of 83.8% after 100 cycles.

ASSOCIATED CONTENT

Supporting Information

The Supporting Information is available free of charge on the ACS Publications website at DOI: 10.1021/acsami.5b11327.

SEM image of SMgO-10 composite and EDX elemental mappings, cyclic voltammograms, initial discharge voltage profiles, discharge capacities, Coulombic efficiencies, AC impedance spectra (PDF)

AUTHOR INFORMATION

Corresponding Author

*E-mail: dongwonkim@hanyang.ac.kr.

Notes

The authors declare no competing financial interest.

ACKNOWLEDGMENTS

This work was supported by the Basic Science Research Program of the National Research Foundation of Korea (NRF), funded by the Ministry of Science, ICT, and Future Planning (2014R1A2A2A01002154). Additional support was provided by the R&D Convergence Program of the National Research Council of Science & Technology (NST) of the Republic of Korea.

REFERENCES

(1) Arico, A. S.; Bruce, P.; Scrosati, B.; Tarascon, J.-M.; van Schalkwijk, W. Nanostructured Materials for Advanced Energy Conversion and Storage Devices. *Nat. Mater.* **2005**, *4*, 366−377.

(2) Tarascon, J. M.; Armand, M. Issues and Challenges Facing Rechargeable Lithium Batteries. *Nature* **2001**, *414*, 359−367.

(3) Manthiram, A.; Fu, Y.; Chung, S. H.; Zu, C.; Su, Y. S. Rechargeable Lithium-Sulfur Batteries. *Chem. Rev.* **2014**, *114*, 11751−11787.

(4) Yin, Y.-X.; Xin, S.; Guo, Y.-G.; Wan, L.-J. Lithium−Sulfur Batteries: Electrochemistry, Materials, and Prospects. *Angew. Chem., Int. Ed.* **2013**, *52*, 13186−13200.

(5) Ji, X.; Nazar, L. F. Advances in Li-S Batteries. *J. Mater. Chem.* **2010**, *20*, 9821−9826.

(6) Bruce, P. G.; Freunberger, S. A.; Hardwick, L. J.; Tarascon, J.-M. Li-O_2 and Li-S Batteries with High Energy Storage. *Nat. Mater.* **2012**, *11*, 19−29.

(7) Li, Z.; Zhang, J. T.; Chen, Y. M.; Li, J.; Lou, X. W. Pie-like Electrode Design for High-Energy Density Lithium−Sulfur Batteries. *Nat. Commun.* **2015**, *6*, 8850.

(8) Manthiram, A.; Chung, S.-H.; Zu, C. Lithium−Sulfur Batteries: Progress and Prospects. *Adv. Mater.* **2015**, *27*, 1980−2006.

(9) Manthiram, A.; Fu, Y.; Su, Y.-S. Challenges and Prospects of Lithium−Sulfur Batteries. *Acc. Chem. Res.* **2013**, *46*, 1125−1134.

(10) Xu, R.; Belharouak, I.; Zhang, X.; Chamoun, R.; Yu, C.; Ren, Y.; Nie, A.; Shahbazian-Yassar, R.; Lu, J.; Li, J. C. M.; Amine, K. Insight into Sulfur Reactions in Li−S Batteries. *ACS Appl. Mater. Interfaces* **2014**, *6*, 21938−21945.

(11) Park, K.; Cho, J. H.; Jang, J.-H.; Yu, B.-C.; De La Hoz, A. T.; Miller, K. M.; Ellison, C. J.; Goodenough, J. B. Trapping Lithium Polysulfides of a Li-S Battery by Forming Lithium Bonds in a Polymer Matrix. *Energy Environ. Sci.* **2015**, *8*, 2389−2395.

(12) Chung, S. H.; Manthiram, A. A Polyethylene Glycol-Supported Microporous Carbon Coating as a Polysulfide Trap for Utilizing Pure Sulfur Cathodes in Lithium-Sulfur Batteries. *Adv. Mater.* **2014**, *26*, 7352−7357.

(13) Ji, X.; Lee, K. T.; Nazar, L. F. A Highly Ordered Nanostructured Carbon-Sulphur Cathode for Lithium-Sulphur Batteries. *Nat. Mater.* **2009**, *8*, 500−506.

(14) Li, D.; Han, F.; Wang, S.; Cheng, F.; Sun, Q.; Li, W.-C. High Sulfur Loading Cathodes Fabricated Using Peapodlike, Large Pore Volume Mesoporous Carbon for Lithium−Sulfur Battery. *ACS Appl. Mater. Interfaces* **2013**, *5*, 2208−2213.

(15) Xin, S.; Gu, L.; Zhao, N.-H.; Yin, Y.-X.; Zhou, L.-J.; Guo, Y.-G.; Wan, L.-J. Smaller Sulfur Molecules Promise Better Lithium−Sulfur Batteries. *J. Am. Chem. Soc.* **2012**, *134*, 18510−18513.

(16) Lee, K. T.; Black, R.; Yim, T.; Ji, X.; Nazar, L. F. Surface-Initiated Growth of Thin Oxide Coatings for Li−Sulfur Battery Cathodes. *Adv. Energy Mater.* **2012**, *2*, 1490−1496.

(17) Moon, S.; Jung, Y. H.; Jung, W. K.; Jung, D. S.; Choi, J. W.; Kim, D. K. Encapsulated Monoclinic Sulfur for Stable Cycling of Li−S Rechargeable Batteries. *Adv. Mater.* **2013**, *25*, 6547−6553.

(18) Cai, K.; Song, M.-K.; Cairns, E. J.; Zhang, Y. Nanostructured Li_2S−C Composites as Cathode Material for High-Energy Lithium/Sulfur Batteries. *Nano Lett.* **2012**, *12*, 6474−6479.

(19) Balach, J.; Jaumann, T.; Klose, M.; Oswald, S.; Eckert, J.; Giebeler, L. Functional Mesoporous Carbon-Coated Separator for Long-Life, High-Energy Lithium-Sulfur Batteries. *Adv. Funct. Mater.* **2015**, *25*, 5285−5291.

(20) Bruckner, J.; Thieme, S.; Bottger-Hiller, F.; Bauer, I.; Grossmann, H. T.; Strubel, P.; Althues, H.; Spange, S.; Kaskel, S. Carbon-Based Anodes for Lithium Sulfur Full Cells with High Cycle Stability. *Adv. Funct. Mater.* **2014**, *24*, 1284−1289.

(21) Zhang, S.; Ueno, K.; Dokko, K.; Watanabe, M. Recent Advances in Electrolytes for Lithium-Sulfur Batteries. *Adv. Energy Mater.* **2015**, *5*, 1500117.

DOI: 10.1021/acsami.5b11327
ACS Appl. Mater. Interfaces 2016, 8, 4000−4006

(22) Wu, F.; Qian, J.; Chen, R.; Lu, J.; Li, L.; Wu, H.; Chen, J.; Zhao, T.; Ye, Y.; Amine, K. An Effective Approach to Protect Lithium Anode and Improve Cycle Performance for Li−S Batteries. *ACS Appl. Mater. Interfaces* **2014**, *6*, 15542−15549.
(23) Ma, G.; Wen, Z.; Wang, Q.; Shen, C.; Jin, J.; Wu, X. Enhanced Cycle Performance of a Li-S Battery Based on a Protected Lithium Anode. *J. Mater. Chem. A* **2014**, *2*, 19355−19359.
(24) Shin, W.-K.; Kannan, A. G.; Kim, D.-W. Effective Suppression of Dendritic Lithium Growth Using an Ultrathin Coating of Nitrogen and Sulfur Codoped Graphene Nanosheets on Polymer Separator for Lithium Metal Batteries. *ACS Appl. Mater. Interfaces* **2015**, *7*, 23700−23707.
(25) Wang, D.-W.; Zeng, Q.; Zhou, G.; Yin, L.; Li, F.; Cheng, H.-M.; Gentle, I. R.; Lu, G. Q. M. Carbon-Sulfur Composites for Li-S Batteries: Status and Prospects. *J. Mater. Chem. A* **2013**, *1*, 9382−9394.
(26) Liang, C.; Dudney, N. J.; Howe, J. Y. Hierarchically Structured Sulfur/Carbon Nanocomposite Material for High-Energy Lithium Battery. *Chem. Mater.* **2009**, *21*, 4724−4730.
(27) Xu, Y.; Wen, Y.; Zhu, Y.; Gaskell, K.; Cychosz, K. A.; Eichhorn, B.; Xu, K.; Wang, C. Confined Sulfur in Microporous Carbon Renders Superior Cycling Stability in Li/S Batteries. *Adv. Funct. Mater.* **2015**, *25*, 4312−4320.
(28) Cheng, H.; Wang, S. Recent Progress in Polymer/Sulphur Composites as Cathodes for Rechargeable Lithium-Sulphur Batteries. *J. Mater. Chem. A* **2014**, *2*, 13783−13794.
(29) Xin, S.; Yin, Y.-X.; Wan, L.-J.; Guo, Y.-G. Encapsulation of Sulfur in a Hollow Porous Carbon Substrate for Superior Li-S Batteries with Long Lifespan. *Part. Part. Sys. Charact.* **2013**, *30*, 321−325.
(30) Ye, H.; Yin, Y.-X.; Xin, S.; Guo, Y.-G. Tuning the Porous Structure of Carbon Hosts for Loading Sulfur toward Long Lifespan Cathode Materials for Li-S Batteries. *J. Mater. Chem. A* **2013**, *1*, 6602−6608.
(31) Wang, J.; Yang, J.; Wan, C.; Du, K.; Xie, J.; Xu, N. Sulfur Composite Cathode Materials for Rechargeable Lithium Batteries. *Adv. Funct. Mater.* **2003**, *13*, 487−492.
(32) Tao, X.; Chen, X.; Xia, Y.; Huang, H.; Gan, Y.; Wu, R.; Chen, F.; zhang, W. Highly Mesoporous Carbon Foams Synthesized by a Facile, Cost-Effective and Template-Free Pechini Method for Advanced Lithium-Sulfur Batteries. *J. Mater. Chem. A* **2013**, *1*, 3295−3301.
(33) Li, X.; Cao, Y.; Qi, W.; Saraf, L. V.; Xiao, J.; Nie, Z.; Mietek, J.; Zhang, J.-G.; Schwenzer, B.; Liu, J. Optimization of Mesoporous Carbon Structures for Lithium-Sulfur Battery Applications. *J. Mater. Chem.* **2011**, *21*, 16603−16610.
(34) Zhang, B.; Qin, X.; Li, G. R.; Gao, X. P. Enhancement of Long Stability of Sulfur Cathode by Encapsulating Sulfur into Micropores of Carbon Spheres. *Energy Environ. Sci.* **2010**, *3*, 1531−1537.
(35) Chen, S.-R.; Zhai, Y.-P.; Xu, G.-L.; Jiang, Y.-X.; Zhao, D.-Y.; Li, J.-T.; Huang, L.; Sun, S.-G. Ordered Mesoporous Carbon/Sulfur Nanocomposite of High Performances as Cathode for Lithium−Sulfur Battery. *Electrochim. Acta* **2011**, *56*, 9549−9555.
(36) Wei Seh, Z.; Li, W.; Cha, J. J.; Zheng, G.; Yang, Y.; McDowell, M. T.; Hsu, P.-C.; Cui, Y. Sulphur−TiO_2 Yolk−Shell Nanoarchitecture with Internal Void Space for Long-Cycle Lithium−Sulphur Batteries. *Nat. Commun.* **2013**, *4*, 1331.
(37) Ji, L.; Rao, M.; Zheng, H.; Zhang, L.; Li, Y.; Duan, W.; Guo, J.; Cairns, E. J.; Zhang, Y. Graphene Oxide as a Sulfur Immobilizer in High Performance Lithium/Sulfur Cells. *J. Am. Chem. Soc.* **2011**, *133*, 18522−18525.
(38) Zhou, G.; Yin, L.-C.; Wang, D.-W.; Li, L.; Pei, S.; Gentle, I. R.; Li, F.; Cheng, H.-M. Fibrous Hybrid of Graphene and Sulfur Nanocrystals for High-Performance Lithium−Sulfur Batteries. *ACS Nano* **2013**, *7*, 5367−5375.
(39) Qiu, Y.; Li, W.; Zhao, W.; Li, G.; Hou, Y.; Liu, M.; Zhou, L.; Ye, F.; Li, H.; Wei, Z.; Yang, S.; Duan, W.; Ye, Y.; Guo, J.; Zhang, Y. High-Rate, Ultralong Cycle-Life Lithium/Sulfur Batteries Enabled by Nitrogen-Doped Graphene. *Nano Lett.* **2014**, *14*, 4821−4827.
(40) Wang, Z.; Dong, Y.; Li, H.; Zhao, Z.; Bin Wu, H.; Hao, C.; Liu, S.; Qiu, J.; Lou, X. W. Enhancing Lithium−Sulphur Battery Performance by Strongly Binding the Discharge Products on Amino-Functionalized Reduced Graphene Oxide. *Nat. Commun.* **2014**, *5*, 5002.
(41) Li, Z.; Zhang, J.; Lou, X. W. Hollow Carbon Nanofibers Filled with MnO_2 Nanosheets as Efficient Sulfur Hosts for Lithium−Sulfur Batteries. *Angew. Chem., Int. Ed.* **2015**, *54*, 12886−12890.
(42) Ji, X.; Evers, S.; Black, R.; Nazar, L. F. Stabilizing Lithium−Sulphur Cathodes Using Polysulphide Reservoirs. *Nat. Commun.* **2011**, *2*, 325.
(43) Campbell, B.; Bell, J.; Bay, H. H.; Favors, Z.; Ionescu, R.; Ozkan, C. S.; Ozkan, M. SiO_2-Coated Sulfur Particles with Mildly Reduced Graphene Oxide as a Cathode Material for Lithium-Sulfur Batteries. *Nanoscale* **2015**, *7*, 7051−7055.
(44) Choi, Y. J.; Jung, B. S.; Lee, D. J.; Jeong, J. H.; Kim, K. W.; Ahn, H. J.; Cho, K. K.; Gu, H. B. Electrochemical Properties of Sulfur Electrode Containing Nano Al_2O_3 for Lithium/Sulfur Cell. *Phys. Scr.* **2007**, *T129*, 62−65.
(45) Evers, S.; Yim, T.; Nazar, L. F. Understanding the Nature of Absorption/Adsorption in Nanoporous Polysulfide Sorbents for the Li−S Battery. *J. Phys. Chem. C* **2012**, *116*, 19653−19658.
(46) Song, M.-S.; Han, S.-C.; Kim, H.-S.; Kim, J.-H.; Kim, K.-T.; Kang, Y.-M.; Ahn, H.-J.; Dou, S. X.; Lee, J.-Y. Effects of Nanosized Adsorbing Material on Electrochemical Properties of Sulfur Cathodes for Li/S Secondary Batteries. *J. Electrochem. Soc.* **2004**, *151*, A791−A795.
(47) Pang, Q.; Kundu, D.; Cuisinier, M.; Nazar, L. F. Surface-Enhanced Redox Chemistry of Polysulphides on a Metallic and Polar Host for Lithium-Sulphur Batteries. *Nat. Commun.* **2014**, *5*, 4759.
(48) Liang, X.; Hart, C.; Pang, Q.; Garsuch, A.; Weiss, T.; Nazar, L. F. A Highly Efficient Polysulfide Mediator for Lithium−Sulfur Batteries. *Nat. Commun.* **2015**, *6*, 5682.
(49) Ning, G.; Liu, Y.; Wei, F.; Wen, Q.; Luo, G. Porous and Lamella-Like Fe/Mgo Catalysts Prepared under Hydrothermal Conditions for High-Yield Synthesis of Double-Walled Carbon Nanotubes. *J. Phys. Chem. C* **2007**, *111*, 1969−1975.
(50) Cornu, D.; Petitjean, H.; Costentin, G.; Guesmi, H.; Krafft, J.-M.; Lauron-Pernot, H. Influence of Natural Adsorbates of Magnesium Oxide on Its Reactivity in Basic Catalysis. *Phys. Chem. Chem. Phys.* **2013**, *15*, 19870−19878.
(51) Coustet, V.; Jupille, J. Hydroxyl Groups on Oxide Surfaces. *Nuovo Cimento Soc. Ital. Fis., D* **1997**, *19*, 1657−1664.
(52) Aramendia, M. A.; Benitez, J. A.; Borau, V.; Jimenez, C.; Marinas, J. M.; Ruiz, J. R.; Urbano, F. Study of MgO and Pt/MgO Systems by XRD, TPR, and ^{1}H MAS NMR. *Langmuir* **1999**, *15*, 1192−1197.
(53) Ardizzone, S.; Bianchi, C. L.; Fadoni, M.; Vercelli, B. Magnesium Salts and Oxide: An XPS Overview. *Appl. Surf. Sci.* **1997**, *119*, 253−259.

DOI: 10.1021/acsami.5b11327
ACS Appl. Mater. Interfaces 2016, 8, 4000−4006